Fomalhaut's debris disc is not dominated by primordial Plutos

Tim D. Pearce[1]⋆, Torsten Löhne[2], Alexander V. Krivov[2]

[1]*Department of Physics, University of Warwick, Gibbet Hill Road, Coventry CV4 7AL, UK*

[2] *Astrophysikalisches Institut und Universitätssternwarte, Friedrich-Schiller-Universität Jena, Schillergäßchen 2–3, 07745 Jena, Germany*

ABSTRACT

A key challenge in debris-disc science is that we do not know the masses of debris discs, nor the sizes of the largest debris bodies. This is because modern observations can only detect objects up to centimetre sizes, whilst larger planetesimals, which dominate disc mass, remain hidden. We must therefore use other arguments, such as dynamics, to indirectly infer disc masses and body sizes. This paper presents a new method, applicable to narrow debris discs like Fomalhaut. We argue that such discs cannot be too massive, nor the largest bodies too large, otherwise they would self-scatter and the disc would be much broader than observed. Using n-body dynamics and collisional theory, we demonstrate that the mass of Fomalhaut's disc cannot be dominated by primordial Plutos. Instead, if the mass is dominated by primordial bodies, then they should have radii below 300^{+80}_{-70} km (0.3 ± 0.1 $R_{\rm Pluto}$) and above 5^{+20}_{-4} km. Our conclusions are robust to additional physics, including shepherding planets and collisional damping. Our results provide independent, dynamical support for the idea that the masses of bright debris discs are dominated by objects smaller than Pluto.

Key words: circumstellar matter – planets and satellites: dynamical evolution and stability

1 INTRODUCTION

Debris discs are circumstellar populations of planetesimals and dust, akin to the Asteroid Belt and Kuiper Belt in our Solar System[1]. These discs are detected around ~ 20 per cent of main-sequence stars, through observations of dust in thermal emission or scattered light (Trilling et al. 2008; Montesinos et al. 2016; Sibthorpe et al. 2018). This dust should only survive for a fraction of the stars' ages before being removed by various physical processes, so it is believed that debris discs also contain larger planetesimals, which continually replenish dust via destructive collisions (Harper et al. 1984; Weissman 1984).

A major problem in debris science is that we cannot directly detect these larger planetesimals around other stars. This is because modern instruments are only sensitive to debris smaller than a few centimetres (Hughes et al. 2018), so we do not know the sizes or quantities of the largest bodies in extrasolar debris discs. However, these largest bodies are key to the dynamical and collisional evolution of debris discs, and should dominate their mass. This means that, despite being a fundamental component of planetary systems, *we do not know how massive extrasolar debris discs are*.

Previous attempts to estimate debris-disc masses involved taking the mass of observed dust (typically ~ 10^{-2} to 10^{-1} $M_\oplus$; Matrà et al. 2025), then extrapolating it up to an arbitrary maximum debris-body size (e.g. planetesimals or Plutos) assuming a theoretical size distribution (e.g. Dohnanyi 1969). However, these estimates are extremely

unreliable, for two reasons. First, we do not know how large the largest debris bodies are; this means we do not know where to stop the extrapolation. Second, there is considerable uncertainty on the form of the size distribution (e.g. Najita et al. 2022), and since the extrapolation can occur over a vast size range, even a slight deviation from the assumed size distribution can lead to huge errors in derived masses.

Furthermore, an inescapable issue has emerged known as the 'debris-disc mass problem'. If the largest extrasolar debris bodies are hundreds or thousands of kilometres in size, as in our Kuiper Belt (and as predicted by planetesimal-formation models), then many of the brightest extrasolar discs would have extrapolated masses exceeding 1000 $M_\oplus$ (Krivov et al. 2018). These values are implausibly high, because they exceed the total solid content thought to be inheritable from protoplanetary discs. The most probable solution is that the brightest debris discs comprise bodies no larger than a few kilometres, which is much smaller than the 1000 km radius of Pluto (Krivov & Wyatt 2021). However, this has not been independently proven.

To proceed, the community needs direct measurements of debris-disc masses and largest-body sizes, which do not rely on extrapolated dust masses. There is no single method for every disc; instead, there are multiple potential methods, each applicable to a subset of discs. Here we present a new method, applicable to narrow discs like Fomalhaut. The idea is that neither the disc mass, nor the size of the largest debris, can be too large, or the disc would scatter itself apart. We use n-body simulations and analytics to demonstrate that Fomalhaut's disc cannot be dominated by 'primordial' Plutos, i.e. ~ 1000 km bodies that formed early in the system's lifetime, otherwise the narrow debris disc would have quickly scattered into a broader shape.

In this paper we consider the Fomalhaut system, owing to its well-

---

⋆ E-mail: tim.pearce@warwick.ac.uk

[1] For reviews of debris discs, see Pearce (2024); Marino (2022); Wyatt (2020); Hughes et al. (2018); Matthews et al. (2014); Krivov (2010); Wyatt (2008).

resolved, narrow debris disc. Fomalhaut A (α PsA; hereafter Fomalhaut) is a 440 ± 40 Myr old A3V star, located at 7.70 ± 0.03 pc (van Leeuwen 2007; Mamajek 2012). Its narrow debris disc has a moderate global eccentricity of ~ 0.1, which is well resolved at multiple wavelengths by the *Hubble Space Telescope*, the Atacama Large Millimeter/submillimeter Array (ALMA), and the *James Webb Space Telescope* (Kalas et al. 2013; MacGregor et al. 2017; Matrà et al. 2017; Gáspár et al. 2023). The origin of the eccentricity is unclear, because the disc is narrower than expected if it started circular and was later sculpted by an eccentric planet (Faramaz et al. 2014; Pearce & Wyatt 2014; Kennedy 2020). The system also hosts the enigmatic object Fomalhaut b, on a highly eccentric and potentially disc-crossing trajectory (Kalas et al. 2013; Pearce et al. 2015). The object was first hypothesised as a planet (Kalas et al. 2008), but its lack of thermal emission precluded it from having high mass (Janson et al. 2012), and such an object would disrupt the disc (Beust et al. 2014) unless in mean-motion resonance with it (Pearce et al. 2021). However, later imaging showed Fomalhaut b to fade with time, suggesting that it is actually a transient, expanding dust cloud (Gáspár & Rieke 2020). Regardless the nature of Fomalhaut b, and how disc attained its narrow, eccentric shape, the disc mass and largest-debris size cannot be too large or the disc would scatter itself apart.

The layout of this paper is as follows. Section 2 describes our *n*-body simulations, showing how discs broaden as a function of disc mass and planetesimal size. Section 3 provides an analytic prediction of disc broadening, and Section 4 combines these dynamical results with collisional theory. Section 5 validates our findings by considering various *caveats* and additional physics. Section 6 considers our results in the wider context of debris-disc science, and we conclude in Section 7.

2 *N*-BODY SIMULATIONS

We test different combinations of disc mass and largest-debris size for the Fomalhaut disc, and for each combination, assess whether the disc could maintain its narrow shape. We first do this with *n*-body simulations; Section 2.1 describes the *n*-body setup, Section 2.2 how the simulations are analysed, and Section 2.3 the results. We later use dynamical theory and secular-ring simulations to extend these *n*-body results to smaller bodies (Section 3 and Appendix B).

2.1 Setup of *n*-body simulations

We perform *n*-body simulations using REBOUND (Rein & Liu 2012). These comprise the Fomalhaut star, and a disc of equal-size, collisional, self-gravitating debris bodies. The debris orbits are initialised to match the observed ALMA disc, using the method in Section 2.1.1 and the system parameters in Table 1.

Each simulation tests a different combination of disc mass m_{disc} and debris-body size s_{max}. The smallest disc mass tested is 0.03 $M_\oplus$ (just above the observed 1 mm dust mass of 0.015 ± 0.010 $M_\oplus$; MacGregor et al. 2017), and the largest 10^4 $M_\oplus$ (above the 10^3 $M_\oplus$ maximum mass in solids thought inheritable from protoplanetary discs; Krivov & Wyatt 2021). Each body's mass is set by equally dividing the disc mass between the number of bodies, where we test between 3 and 10^4 bodies. The body sizes are then calculated from a size-dependent bulk density (Section 2.1.2), and range from 440 km (0.37 R_{Pluto}) up to unphysically large values above 10^4 km for completeness.

Table 1. Parameters of the Fomalhaut system used in this paper. References: [1] Mamajek (2012); [2] van Leeuwen (2007); [3] MacGregor et al. (2017); [4] Grant Kennedy's sdb library[3]. The disc parameters from MacGregor et al. (2017) are all within 3σ of those from more-recent analyses (Chittidi et al. in prep.; Lovell et al. in prep).

Parameter	Name	Value	Unit	Reference
Star parameters				
m_*	Mass	1.92 ± 0.02	$M_\odot$	[1]
L_*	Luminosity	16.63 ± 0.48	$L_\odot$	[1]
t_*	Age	440 ± 40	Myr	[1]
d	Distance	7.70 ± 0.03	pc	[2]
Disc parameters				
a_{disc}	Semimajor-axis median	136.3 ± 0.9	au	[3]
Δa_{disc}	Semimajor-axis range	12.2 ± 1.6	au	[3]
e_{f}	Forced eccentricity	0.12 ± 0.01		[3]
e_{p}	Proper eccentricity	0.06 ± 0.04		[3]
i_{disc}	Midplane inclination to sky	65.6 ± 0.3	deg	[3]
PA	Position angle on sky	337.9 ± 0.3	deg	[3]
ω_{f}	Forced argument of pericentre	22.5 ± 4.3	deg	[3]
m_{dust}	Mass in 1 mm dust grains	0.015 ± 0.010	$M_\oplus$	[3]
f	Fractional luminosity	$(5.3 \pm 0.1) \times 10^{-5}$		[4]
h	Vertical-aspect ratio	0.01 ± 0.01		Assumed
γ	Surface-density index	-1.5		Assumed
ALMA-observation parameters				
λ	Observation wavelength	1.3	mm	[3]
b_{maj}	Synthesized beam major axis	1.56	$''$	[3]
b_{min}	Synthesized beam minor axis	1.15	$''$	[3]
$\mathrm{PA_b}$	Synthesized beam PA	-87	deg	[3]

2.1.1 Initial orbits and positions

We initialise the debris orbits using the fit to the Fomalhaut disc from ALMA observations (Table 1; MacGregor et al. 2017). This model populates orbits based on free- and forced-eccentricities, which are dynamical concepts describing eccentric discs[4]. For each debris body, we randomly draw its semimajor axis a in the range 130.2 to 142.4 au, assuming the surface density scales as $\Sigma \propto a^{-1.5}$ like the Minimum-Mass Solar Nebula (MMSN; Weidenschilling 1977; Hayashi 1981). We uniformly draw its proper longitude of pericentre in the range 0 to 360 deg which, combined with a forced eccentricity e_{f} and proper eccentricity e_{p} (taken as the observed-disc values), yields the debris eccentricity e and the longitude of pericentre ϖ. We use a similar technique to initialise the inclination i and longitude of ascending node Ω, assuming a forced inclination of 0 and a proper inclination of $i_{\mathrm{p}} = \sqrt{2}h$ radians, where h is the assumed vertical-aspect ratio of 0.01 ± 0.01 (based on Boley et al. 2012). Finally, we set the body's initial position on its orbit by uniformly drawing its mean anomaly between 0 and 360 deg. These initial conditions are shown for an example simulation on Figure 1.

2.1.2 Bulk densities of debris bodies

Given a debris body's size, we calculate its mass assuming a spherical shape and a size-dependent bulk density. This size dependence arises because larger bodies can gravitationally compact and differentiate.

---

[3] http://www.drgmk.com/sdb/

[4] A narrow disc like Fomalhaut can be approximated as having a single forced eccentricity e_{f}, and a spread of particle eccentricities around e_{f} set by the proper eccentricity e_{p}.
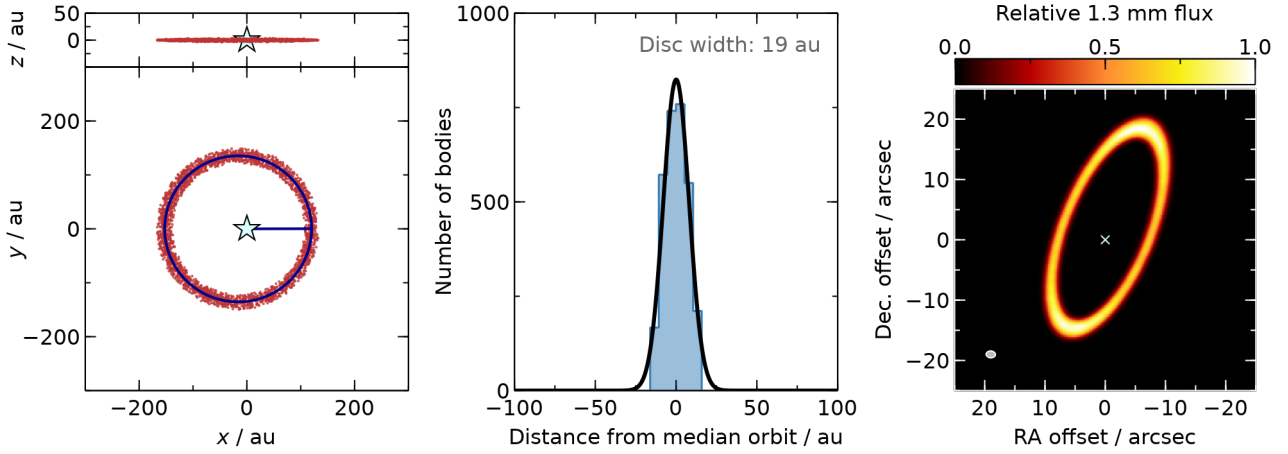
Figure 1. Example setup of an *n*-body simulation. This particular disc has total mass 1 $M_\oplus$, and comprises 3000 debris bodies, each of radius 620 km (0.52 R_{Pluto}). The simulation is shown at time 0, although for these parameters the disc maintains its shape for the whole 440 Myr age of Fomalhaut. *Left*: positions of bodies. The star is at the origin, and each brown point is a debris body. The blue ring is the median debris orbit, and the straight blue line shows the pericentre direction of the median orbit. *Middle*: distances of debris bodies from the median orbit (blue bars). The black line is a Gaussian fit. *Right*: simulated 1.3 mm ALMA image of the *n*-body disc. The cross marks the star, and the oval in the bottom left represents the ALMA beam from MacGregor et al. (2017).

As a proxy, we take the bulk densities of various solid bodies in the Solar System, and fit by eye a simple function for bulk density ρ as a function of body radius s (see Appendix A):

$$\frac{\rho(s)}{\text{g cm}^{-3}} \approx \begin{cases} 0.8 & \text{if } s < 100 \text{ km}; \\ 0.08\sqrt{\frac{s}{\text{km}}} & \text{else.} \end{cases} \quad (1)$$

We use this to relate debris masses and sizes in our *n*-body simulations.

2.1.3 Close approaches

It is necessary to implement either collisions or softening in self-gravitating *n*-body simulations, to prevent particles making unphysically close approaches and receiving unreasonably large velocity kicks. However, a full collisional-fragmentation prescription is far beyond any *n*-body simulation. Instead we model close approaches using a simple hard-sphere model, where colliding particles rebound off each other to a degree that depends on their coefficient of restitution ε. This coefficient lies between 0 and 1, where 1 is a perfectly elastic collision (bodies rebound in opposite directions with no loss of speed), and 0 is a perfectly inelastic collision (bodies effectively stick together). We use a coefficient of restitution that varies with collision speed v_{col} (Bridges et al. 1984), as often used in simulations of planetary rings (e.g. Ohtsuki 1999; Salo et al. 2018):

$$\varepsilon = \min\left[0.109\left(\frac{v_{\text{col}}}{\text{m s}^{-1}}\right)^{-0.234}, 1\right]. \quad (2)$$

For typical collision speeds in debris discs ($\gtrsim 10$ m s^{-1}; Costa et al. 2024), Equation 2 yields a coefficient of restitution close to 0 (inelastic collisions). Our *n*-body simulations therefore incorporate maximal collisional damping between equal-size particles, and if such collisions occurred, our simulated particles would effectively stick together. However, we find damping to be negligible in our simulations, owing to very low collision frequencies.

In reality, collisional debris follows a size distribution, with smaller bodies vastly outnumbering larger ones (Dohnanyi 1969). In certain

regimes, collisions between unequal-sized bodies could significantly damp the larger object (Jankovic et al. 2024), which is unavoidably neglected in our single-size *n*-body simulations. However, in Section 5.1 we will show that realistic collisional damping is negligible in our parameter space of interest, which justifies its omission from our simulations.

2.1.4 Running n-body simulations

Each simulation uses one of two *n*-body prescriptions, depending on the number of bodies *n*. For smaller numbers of particles ($n < 3000$), simple *n*-body gravity is used, where each body feels the exact gravitational force from every other body; in this case the computational requirements scale as n^2. These simulations use REBOUND's MERCURIUS integrator (Rein et al. 2019), which employs the fixed-timestep WHFAST integrator when bodies are far apart, and switches to the IAS15 adaptive-stepsize integrator for close approaches. For these simulations we set WHFAST's timestep to be $10^{-3}P_{0,\text{min}}$, where $P_{0,\text{min}}$ is the orbital period of the innermost particle at the start of the simulation. We also constrain the IAS15 adaptive timestep to not drop below $10^{-9}P_{0,\text{min}}$. Both timesteps are chosen to ensure high accuracy in scattering interactions, exceeding the accuracy of previous works (e.g. Pearce et al. 2024). Collisions are detected using the LINE algorithm.

Conversely, for larger numbers of particles ($n \geq 3000$), we use tree gravity. The physical space is divided into cells, and forces between distant particles are approximated as the total of all particles in a cell. If particles are too close, then cells are subdivided until sufficient accuracy is achieved (Rein & Liu 2012). The computational requirements scale as $n \ln(n)$, so tree gravity is considerably faster than *n*-body gravity for large numbers of particles. For tree simulations we use REBOUND's LEAPFROG fixed-timestep integrator, with a timestep of $10^{-4}P_{0,\text{min}}$. The box size is 3000 au, and particles leaving this box are removed from the simulation. The parameter `opening_angle2`, which sets the tree-code accuracy, is set to 1.5 as in the REBOUND

tree-code example[5, 6]. These computational parameters are chosen as a balance of speed and accuracy based on convergence testing, and verified against *n*-body gravity in Appendix C. Collisions are detected using the LINE-TREE algorithm.

All simulations are either run for the 440 Myr age of Fomalhaut, or until the disc width increases by a factor of 5, whichever occurs first (disc widths are calculated using the method in Section 2.2). This time cutoff is justified because we find that a disc, once broadened, will not coalesce back into a narrow ring through self-gravity; we show this in Appendix B. Furthermore, in Section 5.1 we will show that realistic collisional damping is unlikely to change this.

2.2 Analysis of *n*-body simulations

To quantify how the Fomalhaut disc broadens, we fit the belt width at the end of the simulation, and compare it to the initial width. We describe the fitting process here.

Since the disc is eccentric, we cannot derive its width using an axisymmetric radial profile. Instead, we first calculate the 'median' debris orbit. We define this orbit's semimajor axis as the median of the debris bodies, and set its inclination to zero relative to the disc midplane. Its eccentricity and longitude of pericentre are set by finding the median eccentricity vector of the debris bodies, ($e \cos \varpi$, $e \sin \varpi$). An example of this median orbit is the blue ellipse on the left panel Figure 1.

We then calculate the distance between each debris body and the median orbit, by sampling the median orbit and finding the point closest to the debris body[7]. The middle panel of Figure 1 shows a histogram of these distance for that simulation. Finally, we fit the histogram with a Gaussian (line on the middle panel of Figure 1), and define the disc width as the Gaussian's full-width-half-maximum.

To reduce the effect of random noise, if there are fewer than 100 particles in a simulation, then before calculating the disc width we populate each orbit with 100 pseudo-particles at uniformly randomised mean anomalies. We also run each of those simulations at least 10 times with different seeds, then take the median width.

The right panel of Figure 1 shows a simulated 1.3 mm ALMA observation of the example *n*-body disc, for illustration only. To generate this image, we took each debris body and treated it like a collection of 1.3 mm dust grains. We populated each orbit with 100 pseudo-grains at uniformly random mean anomalies, then calculated each pseudo-grain's temperature as proportional to $r^{-1/2}$ (where r is distance from the star). We then used this temperature to calculate the grain's relative blackbody emission. Finally we rotated the simulation to the system orientation on the sky, and convolved the emission at each point with a 2-dimensional rotated Gaussian representing the ALMA beam of MacGregor et al. (2017). These images are not used in our quantitative analyses.

2.3 Results of *n*-body simulations

Some discs in our *n*-body simulations maintain their narrow, eccentric shape for the 440 Myr age of Fomalhaut. This includes the example on Figure 1. Other discs scatter themselves into much broader structures that are incompatible with observations, like that on Figure 2. The broadening time varies between simulations, but in many simulations it is orders-of-magnitude shorter than the system age.

Figure 3 shows the results of all *n*-body simulations. Each cross marks a simulation, and the colourmap shows how much the simulated discs broaden. There is a clear divide between behaviours; if a disc is too massive, or the bodies too large, then the disc scatters into a broader structure (upper-right region of Figure 3). Conversely, if the disc mass and/or body size is small, the disc maintains its narrow shape across the system age. Disc mass alone does not decide this behaviour; for a given disc mass, discs with smaller bodies are better able to remain narrow (e.g. the 10 $M_\oplus$ discs on Figure 3). In Section 3 we will verify these results using dynamical theory.

Our initial-disc widths are 19 au, which are wider than the synthesised ALMA beam; the beam has major axis $1.56'' \times 7.7$ pc = 12 au, and minor axis $1.15'' \times 7.7$ pc = 8.9 au (MacGregor et al. 2017). This means that the initial belt, which matches observations, is resolved by 1.6 to 2.1 beams at its ansae. We conservatively argue that we can rule out simulations where the disc broadens by more than a factor of 1.5, because this difference would be detectable in ALMA observations. This suggests that we can already rule out largest-debris sizes above ~ 4 R_{Pluto}, based on Figure 3, because larger bodies would significantly broaden the disc. However, we will produce tighter constraints in Section 4, by combining our dynamical arguments with collisional theory.

These results assume that the initial disc had the same width as the observed disc. This is valid for two reasons. First, the disc is unlikely to have be born wider and then narrowed, for the reasons given in Appendix B. Second, if the initial disc were narrower, then the initial number density of particles would have been higher, so scattering would be more efficient and the disc would broaden even more. In Section 3 we will show that the eccentricity of self-scattering bodies grows faster for narrower discs, so narrow initial discs would broaden faster. This means that our upper limits on disc mass and largest-body size still apply, even if the initial disc were narrower.

3 THEORETICAL PREDICTION OF DISC BROADENING

We now use dynamical theory to predict the disc masses and debris sizes required to significantly broaden a narrow disc. This verifies our *n*-body simulations, and provides general predictions applicable to other systems.

Ida & Makino (1993) quantify the viscous-stirring timescale for a disc of self-stirring planetesimals. They start with an axisymmetric disc of equal-mass planetesimals, with low initial eccentricities and inclinations, and quantify how the root-mean-square eccentricity $\sqrt{\langle e^2 \rangle}$ grows with time t. Combining their Equations 4.1 and 4.2, and deriving their surface-number density of planetesimals using the disc width w_{disc}, yields

$$\sqrt{\langle e^2 \rangle} = \left(\frac{2}{3} \frac{C_{\mathrm{e}} \sqrt{G} s^3 \rho m_{\mathrm{disc}}}{m_*^{3/2} \sqrt{a_{\mathrm{disc}}} w_{\mathrm{disc}}} t \right)^{\frac{1}{4}} \tag{3}$$
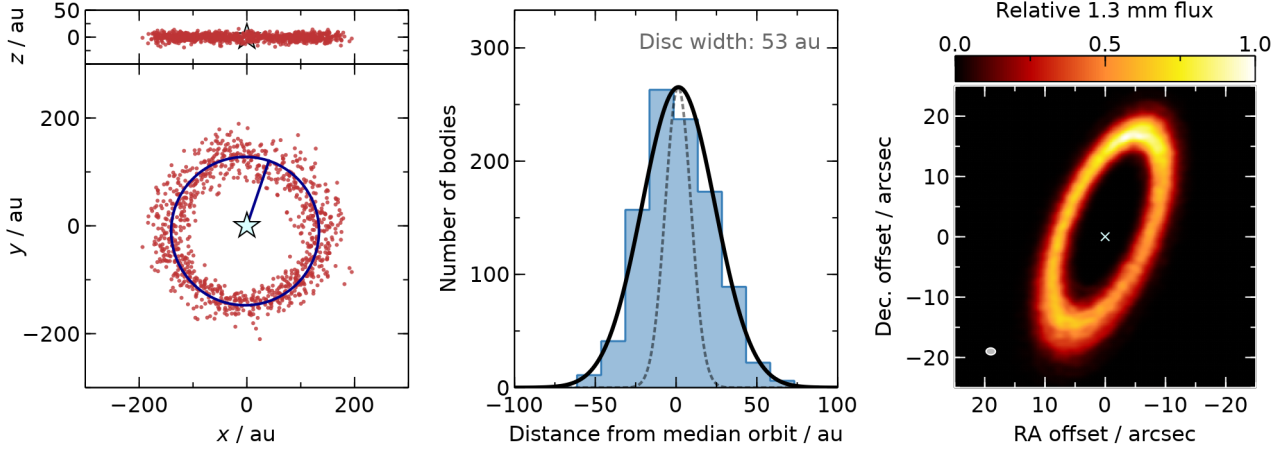
or equivalently

Figure 2. Example *n*-body simulation where the disc significantly broadens via self-scattering. This disc has a total mass of 30 $M_\oplus$, and comprises 1000 debris bodies each of radius 2200 km (1.9 R_{Pluto}). This simulation started in a similar configuration to Figure 1, and is shown after 160 Myr; by this time the disc has almost tripled in width, and is incompatible with observations. Definitions and most axis scales are the same as Figure 1, although the histogram vertical axis has been rescaled due to the different number of bodies, and the flux on the right panel has a different normalisation. The dotted line on the middle panel shows the disc profile at the start of the simulation.
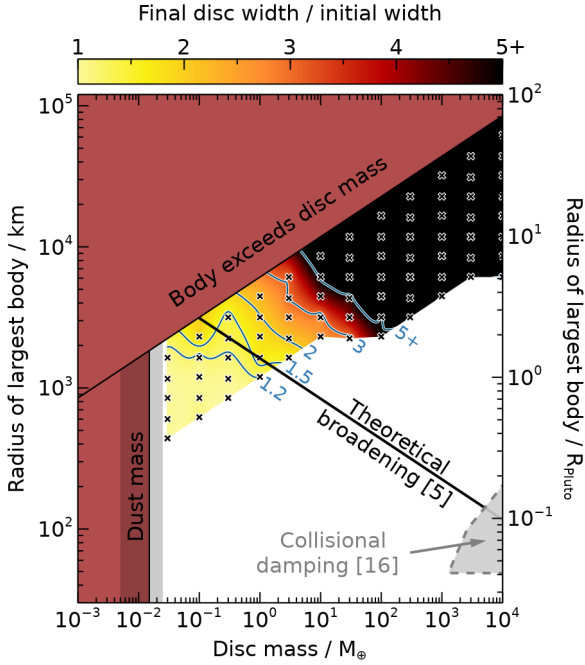

Figure 3. Expected broadening of Fomalhaut's debris disc, as a function of disc mass and the size of the largest debris bodies. Crosses mark *n*-body simulations. The colour scale and contour lines show the interpolated final width of those simulated discs, divided by their initial widths. Discs that are too massive, or made up of bodies that are too large, readily scatter into broader structures (upper-right region). Red blocked areas are unphysical; the total disc mass must be larger than that in observed millimetre dust (left), and one body cannot be more massive than the whole disc (top). The 'Theoretical broadening' line is our prediction, above which a narrow planetesimal disc would significantly widen through self scattering (Equation 5). The 'Damping' area is where realistic collisional damping could cause the disc to narrow (Equation 16). Numbers in square brackets denote equations, and the shading around the 'Dust mass' line is the observational uncertainty (Table 1).

$$\sqrt{\langle e^2 \rangle} = 1.261 \times 10^{-4} \left(\frac{C_e}{40}\right)^{\frac{1}{4}} \left(\frac{s}{\mathrm{km}}\right)^{\frac{3}{4}} \left(\frac{\rho}{\mathrm{g\ cm^{-3}}}\right)^{\frac{1}{4}} \left(\frac{m_{\mathrm{disc}}}{M_\oplus}\right)^{\frac{1}{4}}$$
$$\times \left(\frac{a_{\mathrm{disc}}}{\mathrm{au}}\right)^{-\frac{1}{8}} \left(\frac{w_{\mathrm{disc}}}{\mathrm{au}}\right)^{-\frac{1}{4}} \left(\frac{m_*}{M_\odot}\right)^{-\frac{3}{8}} \left(\frac{t}{\mathrm{Myr}}\right)^{\frac{1}{4}}, \quad (4)$$

where $C_e \sim 40$ is a numerical constant (Ida & Makino 1993)[8].

Applying this to Fomalhaut: a ring of particles with semimajor axis a_{disc}, forced eccentricity e_{f} and proper eccentricity e_{p} has a width $w_{\mathrm{disc}} = 2a_{\mathrm{disc}}e_{\mathrm{p}}$. Hence Fomalhaut's disc would be significantly wider if the root-mean-square eccentricities from self scattering were greater than $w_{\mathrm{disc}}/(2a_{\mathrm{disc}})$. So rearranging Equation 4 yields the maximum initial mass the narrow disc could have, as a function of largest-debris size, without significantly broadening within the age of the star:

$$\left(\frac{m_{\mathrm{disc},0}}{M_\oplus}\right) \lesssim 2.5 \times 10^{14} \left(\frac{C_e}{40}\right)^{-1} \left(\frac{s}{\mathrm{km}}\right)^{-3} \left[\frac{\rho(s)}{\mathrm{g\ cm^{-3}}}\right]^{-1}$$
$$\times \left(\frac{a_{\mathrm{disc}}}{\mathrm{au}}\right)^{-\frac{7}{2}} \left(\frac{\Delta a_{\mathrm{disc}}}{\mathrm{au}}\right)^5 \left(\frac{m_*}{M_\odot}\right)^{\frac{3}{2}} \left(\frac{t_*}{\mathrm{Myr}}\right)^{-1}. \quad (5)$$

Here we used the semimajor-axis range Δa_{disc} as a proxy for the initial-disc width w_{disc}. In reality the semimajor axes would also spread, which would broaden the ring even more; hence Equation 5 is a firm upper limit on the maximum initial mass a narrow disc could have without significantly broadening.

We plot Equation 5 as the solid black line on Figure 3, using the size-dependent bulk density from Equation 1. The line shows good agreement with our simulations; simulations below the line maintain

---

[8] Equations 3 and 4 are comparable to Equation 11 in Matrà et al. (2019), except that ours apply to planetesimal-planetesimal scattering, rather than planet-planetesimal scattering (so are smaller than Matrà et al. 2019 by a factor of $2^{1/4}$), and ours apply to eccentricity rather than inclination (for inclination, substitute e for i and C_e for $C_i \sim 2$ in Equations 3 and 4; Ida & Makino 1993).
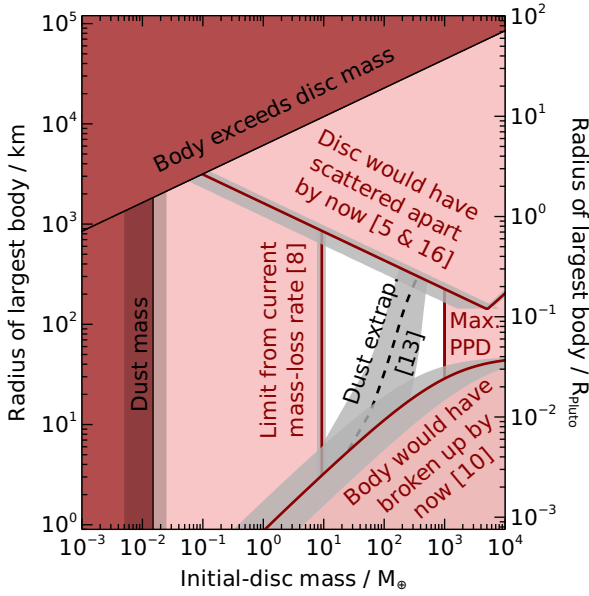
Figure 4. Combined dynamical and collisional constraints on the Fomalhaut debris disc. Red shaded regions are ruled out by physical arguments, with numbers in brackets denoting the corresponding equation numbers. The dashed line is an extrapolation from observed dust; if debris follows the 3-powerlaw size distribution of Löhne et al. (2008), then the total disc mass and largest-body size lies along this line. 'Max. PPD' denotes the 10^3 M$_\oplus$ maximum mass in solids thought inheritable from protoplanetary discs (Krivov & Wyatt 2021). The horizontal axis is the disc's initial mass, but for the top ~two-thirds of the plot (radii > 48 km), the initial-disc mass equals the present-day mass, because the largest bodies have not yet started colliding. Shading around lines denotes 1σ uncertainties, propagated from observational uncertainties in Table 1. Note that the vertical-axis scale is larger than Figure 3.

their narrow shapes, whilst those above the line undergo broaden by a factor of at least 1.3. Equation 5 is therefore a good predictor for the maximum mass a narrow planetesimal disc can have without scattering itself apart.

4 COMBINING DYNAMICS WITH COLLISIONS

Sections 2 and 3 gave purely dynamical constraints on disc mass and largest-body size. However, we get more-powerful constraints by combining dynamics with collisional theory. Here we use several collisional arguments to further constrain the allowed parameter space, with the resulting bounds shown on Figure 4. Using this, we show that the mass of Fomalhaut's debris disc cannot be dominated by primordial Plutos. The arguments are as follows.

4.1 Lower bound on disc mass from mass-loss rate

The disc mass must be larger than the observed-dust mass of 0.015 ± 0.010 M$_\oplus$ (MacGregor et al. 2017), but a more-stringent constraint comes from collisional evolution. Following Krivov & Wyatt (2021), a debris disc in collisional cascade, where bodies are predominantly destroyed by collisions with similar-sized bodies, has mass decreasing with time t as

$$m_{\mathrm{disc}}(t) = \frac{m_{\mathrm{disc},0}}{1 + t/\tau_0}. \tag{6}$$

Here $m_{\mathrm{disc},0}$ is the initial-disc mass, and τ_0 is the collisional lifetime of the largest bodies at the initial epoch (Wyatt et al. 2007; Löhne et al. 2008). Differentiating this, and setting t to the star age t_*, yields

$$m_{\mathrm{disc},0} = |\dot{m}_{\mathrm{disc}}(t_*)|\tau_0 (1 + t_*/\tau_0)^2. \tag{7}$$

Here $|\dot{m}_{\mathrm{disc}}(t_*)|$ is the current mass-loss rate, which can be estimated from observations (see below). The value τ_0 depends on the disc parameters, disc mass, and the largest-body size, but by differentiating Equation 7 with respect to τ_0, we see that the equation is minimised if $\tau_0 = t_*$. Hence a lower bound on the initial-disc mass is

$$m_{\mathrm{disc},0} \gtrsim 4|\dot{m}_{\mathrm{disc}}|t_*. \tag{8}$$

We now apply this to Fomalhaut, using the parameters and uncertainties from Table 1. The mass-loss rate is estimated using Equation 21 in Matrà et al. (2017), yielding $|\dot{m}_{\mathrm{disc}}| = (5.3 \pm 0.7) \times 10^{-3}$ M$_\oplus$ Myr^{-1}. Inserting this into Equation 8 yields a lower bound on the initial-disc mass of 9 ± 2 M$_\oplus$. This limit is shown on Figure 4, and lies comfortably between equivalent lower limits of 3.6 M$_\oplus$ from Krivov & Wyatt (2021) and 19 M$_\oplus$ from Matrà et al. (2017)[9].

By comparing Equations 5 and 8, we see that the largest primordial bodies cannot be Plutos, because in that case the minimum-mass disc would have scattered apart by now. From the intercept of these lines on Figure 4, the largest primordial body must have a radius below $0.7^{+0.1}_{-0.2}$ R$_{\mathrm{Pluto}}$ (800 $\pm$ 100 km).

Equation 8 is a lower bound on the initial-disc mass, but if τ_0 is large enough, then the largest bodies will not yet have started colliding. In this case the present-day disc mass will be the same as its initial mass, and the lower bound of 9 ± 2 M$_\oplus$ from Equation 8 also applies to the present-day disc. As we will show in Section 4.2, this is true regardless of disc mass if the largest body has radius $\gtrsim 48$ km (if made of basalt) or $\gtrsim 250$ km (if made of ice). Also, whilst the lower bound from Equation 8 includes an implicit assumption about the dust-size distribution, in Section 5.2 we show the results are robust for reasonable assumptions.

4.2 Collisional lifetimes of the largest bodies

The second constraint comes from the collisional lifetimes of the largest bodies. A large body's collisional lifetime increases with body size (because larger bodies are stronger), and decreases with disc mass (because more objects means more collisions). So for a given initial-disc mass, there is a lower limit on the size of a primordial body for it to survive until the present day.

We use the collisional prescription of Löhne et al. (2008). This assumes that debris follows a triple-powerlaw size distribution for radii between s_{min} and s_{max}, where $n(s)\mathrm{d}s$ is the number of bodies with radii between s and $s + \mathrm{d}s$, and

$$n(s) \propto \begin{cases} s^{2-3q_{\mathrm{s}}} & \text{if } s_{\mathrm{min}} \leq s < s_{\mathrm{b}}, \\ s^{2-3q_{\mathrm{g}}} & \text{if } s_{\mathrm{b}} \leq s < s_{\mathrm{km}}, \\ s^{2-3q_{\mathrm{p}}} & \text{if } s_{\mathrm{km}} \leq s < s_{\mathrm{max}}, \\ 0 & \text{else.} \end{cases} \tag{9}$$

[9] 3.6 M$_\oplus$ comes from substituting the Krivov & Wyatt (2021) lower bound on the *current* mass (1.8 M$_\oplus$) into Equation 6 with $t = \tau_0$. 19 M$_\oplus$ comes from substituting the Matrà et al. (2017) estimate of $|\dot{m}_{\mathrm{disc}}| = 1.1 \times 10^{-2}$ M$_\oplus$ Myr^{-1} into Equation 8.

Here s_{km} is the radius of the largest *colliding* body, s_{max} the radius of the largest *primordial* body (which has not yet entered the collisional cascade), and s_b the radius of the weakest body (around the size where bodies transition from being held together by material strength to gravity). Following Löhne et al. (2008), we use $q_s = 1.89$, $q_g = 1.68$ and $q_p = 1.87$; these correspond to $n(s) \propto s^{-3.67}$, $s^{-3.04}$ and $s^{-3.61}$ in the three respective regimes. We discuss the impact of uncertainties on these values in Section 5.2.

Equation 42 in Löhne et al. (2008) gives τ_0, the collisional lifetime of the largest body at the initial epoch, as a function of body size s_{max}, initial-disc mass $m_{disc,0}$, and other parameters[10]. However, τ_0 is not necessarily the *actual* collisional lifetime, because over time the disc mass decreases, and hence the collisional lifetime increases. So to get a lower limit on the largest primordial body that could survive until today, we set $\tau_0 = t_*$ and the disc mass to $m_{disc,0}/2$; this is the present-day disc mass if $\tau_0 = t_*$ (Equation 6). We do this because a primordial body that were too small to survive until today with the collisionally reduced disc mass would be even less likely to survive in reality, because the initial-disc mass was even larger. Hence the maximum initial-disc mass that allows the largest body to survive until the present day is

$$m_{disc,0}(s_{max}) < 2 \times \frac{16\pi\rho(s_{max})}{3t_*} \frac{s_{max}a_{disc}^{5/2}\Delta a_{disc}}{\sqrt{\mathcal{G}m_*}}$$
$$\times \frac{q_g - 5/3}{2 - q_p} \left[1 - \left(\frac{s_{min}}{s_{max}} \right)^{6-3q_p} \right] \frac{i}{f(e,i)G(q_g, s_{max}, a_{disc})}. \quad (10)$$

Here $\mathcal{G}$ is the gravitational constant, e and i are the typical relative eccentricities and inclinations of bodies respectively, and the functions $f(e,i)$ and $G(q,s,r)$ are defined in Appendix D.

Equation 10 depends on the material strength Q_D^*, which is contained in $G(q,s,r)$. To make a conservative estimate of the maximum disc mass, we assume debris is composed of strong basalt; weaker materials would break apart sooner, so the disc would have to be even less massive for those bodies to survive. Following Löhne et al. (2012), Schüppler et al. (2016) and Krivov et al. (2018), we use a size-dependent fragmentation energy of

$$Q_D^*(s,r) = \left(\frac{v_{col}}{v_0} \right)^{1/2} \left[A_s \left(\frac{s}{1\,m} \right)^{-3b_s} + A_g \left(\frac{s}{1\,km} \right)^{3b_g} \right], \quad (11)$$

where $v_0 = 3\,km\,s^{-1}$, $A_s = A_g = 5 \times 10^6\,erg\,g^{-1}$, $b_s = 0.12$ and $b_g = 0.46$. For this material, Q_D^* is minimised for bodies with radii equal to the breaking radius $s_b = 110\,m$. The collision speed v_{col} is

$$v_{col} = \sqrt{\frac{\mathcal{G}m_*}{a_{disc}}f(e,I)}. \quad (12)$$

We now apply this to Fomalhaut: we set $e = e_p$ and $i = \sqrt{2}h$, which yields typical collision speeds of $v_{col} \sim 240 \pm 10\,m\,s^{-1}$ in the disc. We arbitrarily set $s_{min} = 1\,\mu m$, and use the size-dependent bulk density $\rho(s)$ from Equation 1. Using these, Equation 10 yields the maximum initial-disc mass as a function of body size, as shown on Figure 4.

We see that, for basalt bodies, anything with radius larger than

~ 48 km is strong enough to never break up in the Fomalhaut disc (i.e. $\tau \to \infty$)[11]. From Equation 6, this means that for the upper $\sim$two-thirds of Figure 4 (radii $\gtrsim 48$ km), the current disc mass equals its initial mass. We also note that this critical size is well below the sizes tested in our *n*-body simulations; hence those bodies would still exist today, and we are safe to omit collisional erosion from our *n*-body simulations[12].

Whilst bodies larger than ~ 48 km would survive indefinitely, smaller primordial bodies could have broken up by now, if the disc were massive enough. Combining Equation 10 with the minimum disc mass from Equation 8, we see that the largest primordial body in Fomalhaut's disc must have had a radius larger than 3^{+2}_{-1} km, otherwise it would already have broken up. Bodies composed of weaker materials would have stricter limits; icy bodies could have A_s and A_g reduced by a factor of 10 in Equation 11 (Krivov et al. 2005), in which case icy primordial bodies would require radii larger than at least 7 km to survive until the present day, and larger for higher disc masses. Similarly, any primordial icy body with radius above ~ 250 km could survive indefinitely, for any mass of the Fomalhaut disc.

4.3 Extrapolating dust mass

The final constraints come from dust mass. If we know the form of the size distribution, then we can estimate the total mass in bodies up to a given size, by extrapolating the mass in observed dust. This technique cannot uniquely constrain disc mass, because we do not know the size of the largest body and hence how far to extrapolate, but it can relate disc mass and largest-body size.

Here we constrain the largest-body size as a function of initial-disc mass $m_{disc,0}$. We do this numerically; for a given initial-disc mass, we interpolate to find the corresponding largest-body size s_{max}. First, we normalise the present-day size distribution (Equation 9) at the smallest sizes. The total mass of spherical bodies with radii between s_1 and s_2 is

$$m_{s_1 \to s_2} = \frac{4\pi}{3} \int_{s_1}^{s_2} n(s)\rho(s)s^3 ds, \quad (13)$$

so we normalise the size distribution from s_{min} to s_b by setting $m_{s_{min} \to s_{dust}} = m_{dust}$.

We then normalise the second part of the size distribution, from s_b to s_{km}, by assuming the distribution is continuous at s_b. The upper end of this part is s_{km}, the radius of the current largest colliding body. This can be found from Equation 31 in Löhne et al. (2008), which gives the collisional lifetime of an object of radius s:

$$\tau = \frac{16\pi\rho(s)}{3m_{disc,0}} \left(\frac{s}{s_{max}} \right)^{3q_p-5} \frac{s_{max}a_{disc}^{5/2}\Delta a_{disc}}{\sqrt{\mathcal{G}m_*}}$$
$$\times \frac{q_p - 5/3}{2 - q_p} \left[1 - \left(\frac{s_{min}}{s_{max}} \right)^{6-3q_p} \right] \frac{i}{f(e,i)G(q_p, s, a_{disc})}. \quad (14)$$

Solving this for s at $\tau = t_*$ yields s_{km}. Bodies larger than s_{km} have

---

[10] Pearce et al. 2024 note that Equation 42 in Löhne et al. (2008) has an erroneous index of -1 around the square bracket, which we omit here. This is unimportant provided $q_p < 2$ and $s_{min} \ll s_{max}$.

[11] The minimum debris size to never break apart is given by Equation 31 in Pearce et al. (2024).

[12] If the disc lost mass through collisional erosion, then dynamical broadening would be reduced. However, this would require the disc parameters to lie in the bottom-right of Figure 4 (below Equation 10), in which case dynamical broadening is negligible anyway. Hence mass loss does not affect our dynamical conclusions.

not yet started colliding, so the size distribution has the primordial slope from $s_{\rm km}$ to $s_{\rm max}$. Again, we normalise this part by assuming the distribution is continuous at $s_{\rm km}$.

Having normalised the *present-day* size distribution at $s_{\rm km}$, we can finally calculate $s_{\rm max}$ as a function of $m_{\rm disc,0}$ by integrating along the *primordial* size distribution (i.e. $m_{s_{\rm min} \to s_{\rm max}} = m_{\rm disc,0}$, integrated over the normalised primordial powerlaw $s^{2-3q_{\rm p}}$). In practise this must be solved numerically, because Equation 14 for $s_{\rm km}$ also depends on $s_{\rm max}$. We therefore iterate to find the $s_{\rm max}$ value that simultaneously yields $s_{\rm km}$ and $m_{\rm disc,0}$.

The result is the dashed line on Figure 4. If the current disc obeys the assumed size distribution (Equation 9), then the initial-disc mass and largest-body size should lie somewhere along this line. The intercept of this line with the dynamical-broadening line from Equation 5 yields upper limits on the initial-disc mass and largest-body size. The initial-disc mass would have to have been below 400 ± 100 $M_\oplus$, and the largest-body radius would have to have been below 300^{+80}_{-70} km (0.3 ± 0.1 $R_{\rm Pluto}$). Such large bodies would not yet have started colliding, so would still exist today with their primordial size distribution. Since these largest bodies dominate the disc mass, this means that, in this case, the disc would still have its original mass today. Similarly, from the intercept of Equation 13 with Equation 10, the largest primordial body must have a radius above 5^{+20}_{-4} km to still survive today.

5 CAVEATS AND ADDITIONAL PHYSICS

We used *n*-body dynamics and collisional theory to argue that Fomalhaut's debris disc cannot be dominated by primordial Plutos. We now show that this conclusion is robust, by checking various caveats and additional physics. Section 5.1 considers the effects of realistic collisional damping, and Section 5.2 examines our assumed size distribution. Section 5.3 considers whether the largest bodies dominate disc mass, and Section 5.4 discusses our omission of planetesimal growth. Sections 5.5 and 5.6 test whether gas drag or shepherding planets would affect our argument.

5.1 Collisional damping by smaller bodies

Our *n*-body simulations comprise bodies of one size with predominantly inelastic collisions, for which collisional damping is negligible. However, real debris follows a size distribution, so larger bodies could be significantly damped by collisions with smaller bodies. Here we use Jankovic et al. (2024) to show that, whilst realistic collisional damping can sometimes prevent disc broadening, this does not occur in our parameter space of interest. Hence our conclusions would remain valid, even considering more-realistic collisional damping.

Jankovic et al. (2024) show that collisional damping is set by both the collisional timescale and the projectile-to-target-mass ratio $Y_{\rm c}$. Given enough time, damping would eventually become important for a body of a given size if

$$Y_{\rm c} = \frac{2Q_{\rm D}^*}{v_{\rm col}^2} \gtrsim 1. \qquad (15)$$

Substituting $v_{\rm col} \sim 240 \pm 10$ m s^{-1} from Equation 12 into Equation 15, and using $Q_{\rm D}^*$ for basalt from Equation 11, we find that millimetre dust is always safe from collisional damping in the Fomalhaut disc ($Y_{\rm c} \sim 0.059 \pm 0.004$). Conversely, larger objects are not; Equation 15 shows that, given enough time, collisional

damping would eventually become important for bodies larger than $\sim 48 \pm 2$ km.

However, the second factor is the damping timescale. Large bodies may eventually be susceptible to damping, but this may take so long that it is unimportant in our regime. Jankovic et al. (2024) quantify the damping timescale for a realistic debris-size distribution. Combining their Equations 2 and 5 shows that, for collisional damping to affect the largest bodies within the star lifetime,

$$m_{\rm disc} \gtrsim 0.01 (4-\alpha)^{-1} \left(\frac{s_{\rm max}}{\rm km}\right)^{4-\alpha} \left[\frac{\rho(s_{\rm max})}{\rm g\ cm^{-3}}\right] \left(\frac{a_{\rm disc}}{\rm au}\right)^{5/2} \left(\frac{\Delta a_{\rm disc}}{\rm au}\right)$$
$$\times \left(\frac{m_*}{\rm M_\odot}\right)^{-1/2} \left(\frac{t_*}{\rm Myr}\right)^{-1} \left[\frac{I(s_{\rm max}, \alpha)}{\rm km^{3-\alpha}}\right]^{-1}, \qquad (16)$$

where α is the size-distribution slope in the region of interest ($n(s){\rm d}s \propto s^{-\alpha}{\rm d}s$), and $I(s_{\rm max}, \alpha)$ is the integral

$$I(s_{\rm t}, \alpha) = \int_{s_{\rm min}}^{s_{\rm max}} s_{\rm p}^{-\alpha}(s_{\rm p} + s_{\rm t})^2 \frac{m_{\rm p}(s_{\rm p})m_{\rm t}(s_{\rm t})}{[m_{\rm p}(s_{\rm p}) + m_{\rm t}(s_{\rm t})]^2}{\rm d}s_{\rm p}. \qquad (17)$$

Here subscripts p and t denote properties of the projectile and target bodies respectively, *s* denotes body radius, *m* denotes body mass, and $s_{\rm min}$ is the smallest projectile to consider. We substitute values for Fomalhaut, assuming a size-distribution index for primordial bodies of $\alpha = 3q_{\rm p} - 2 = 3.61$ (Equation 9), calculating body masses using the size-dependent bulk density of Equation 1, and setting $s_{\rm min} = 1$ mm. The result is the shaded region in the bottom right of Figure 3, which shows only bodies large enough that damping could eventually be important (i.e. $Y_{\rm c} > 1$).

This analysis demonstrates that, whilst large bodies would eventually be susceptible to collisional damping, the damping timescales are generally much longer than Fomalhaut's age. The only region of our parameter space that is susceptible to damping is debris discs with masses above 1000 $M_\oplus$, which is unphysical based on the maximum solid content inheritable from protoplanetary discs (Krivov & Wyatt 2021). We therefore conclude that collisional damping, if it occurs at all, is generally too slow to affect our results. Hence discs that broaden in our *n*-body simulations, often over very short timescales, would not be damped via collisions.

This conclusion is the opposite of Nesvold et al. (2013), who make a pioneering effort to simultaneously model collisions and *n*-body dynamics. They use the collisional *n*-body code SMACK, and infer that collisions can drive broad discs into narrow, eccentric rings like Fomalhaut. They use a superparticle approach, where each superparticle represents a population of debris bodies with a size distribution. However, they only simulate debris sizes up to 10 cm and, since SMACK does not include mass segregation, they argue that their method substantially overestimates collisional damping of larger bodies. They also omit debris mass, and hence the effect of scattering. These reasons could explain why we do not reconcile their results with Jankovic et al. (2024), who show that collisional damping of planetesimals would be negligible in Fomalhaut's disc. We therefore conclude that collisional damping is unlikely to resist scattering-driven broadening, and hence that our conclusions hold, although further work is required to identify exactly why our conclusions differ from Nesvold et al. (2013).

5.2 Assumed size distribution

Our conclusion, that Fomalhaut's disc is not dominated by primordial Plutos, comes from combining dynamical constraints (Equation 5)

with disc-mass constraints (Equation 8). The latter depends on the size distribution around millimetre sizes, because this sets the dust's collisional lifetime and hence the mass-loss rate $\dot{m}_{\text{disc}}$. However, millimetre dust is firmly in the collisional cascade, so its size distribution is well constrained to lie around $n(s) \propto s^{-3.5}$ (e.g. Dohnanyi 1969; Tanaka et al. 1996; Durda & Dermott 1997; O'Brien & Greenberg 2003; Kobayashi & Tanaka 2010; Wyatt et al. 2011; Pan & Schlichting 2012; Vizgan et al. 2022). We assumed $s^{-3.67}$ based on $q_s = 1.89$ from Löhne et al. (2008), but changing this to extreme values of s^{-3} or s^{-4} would only alter our lower bound on initial-disc mass by a factor of 1.7 in either direction (Equation 19 in Matrà et al. 2017). This is not sufficient to let primordial Plutos reside in the Fomalhaut disc (Figure 4).

A less certain parameter is the primordial size distribution, set by q_p. This is often approximated from planetesimal-formation models (e.g. Johansen et al. 2015; Simon et al. 2016, 2017; Abod et al. 2019). However, our main conclusion is robust to q_p, because it does not directly enter Equations 5 or 8. It indirectly comes into Equation 5, by implicitly assuming that the total disc mass is dominated by the largest bodies; however, in Section 5.3 we show that Equations 5 is also robust to the size distribution.

The places where q_p has the biggest influence is the collisional lifetime of the largest bodies (Equation 10), and the extrapolation of dust mass up to total disc mass (Equation 13). We assume $q_p = 1.87$ based on Löhne et al. (2008), which results in $n(s) \propto s^{-3.61}$ for large bodies. However, this is uncertain; for example, Krivov & Wyatt (2021) use $s^{-2.8}$ (i.e. $q_p = 1.6$). To reflect this, we use uncertainties of $q_p = 1.9^{+0.1}_{-0.3}$ to generate the uncertainties on Figure 4. To further test the effect of q_p, we re-run our collisional analyses with an extreme primordial-size distribution of s^{-2}. In this case, the collisional-lifetime line (Equation 10) moves left on Figure 4; the initial-disc mass required for a body to have broken up is reduced by a factor of 5. Also, the dust-extrapolation line (Equation 13) moves right, such that the the initial-disc mass could be as high as 1000 $M_\oplus$ whilst still being consistent with observed dust. In this case the largest-body radius would be below 220 km.

The final parameter is q_g, which sets the size distribution in the gravity regime. Whilst this also affects the collisional lifetime of the largest bodies (Equation 10), and the extrapolation of dust mass (Equation 13), it does not affect Equation 5 or Equation 8. This means it has no effect on our conclusion. In summary, since none of the above changes allow Fomalhaut's disc to contain primordial Plutos, our conclusions seem robust to reasonable assumptions about the size distribution.

5.3 Assumption that the largest bodies dominate disc mass

By dividing the disc mass between the largest bodies in our n-body simulations, we implicitly assumed that the largest bodies dominate disc mass. This is the standard assumption in debris science, and appears reasonable; for example, Pluto and Eris alone hold 25 per cent of the Kuiper Belt's mass (Pitjeva & Pitjev 2018). It is valid if a disc's size distribution $n(s) \propto s^{-\alpha}$ has $\alpha < 4$, which is satisfied for debris in a steady state collisional cascade, for which $\alpha \approx 3.5$ (Dohnanyi 1969). However, in reality the largest bodies may not yet have entered the cascade, and would still have their primordial size distribution (Section 4.2). This primordial distribution is uncertain, so it is not clear that the largest bodies in a disc really dominate its mass.

Bodies up to several hundred kilometres in size are thought to form with $\alpha < 4$, based on planetesimal-formation models (Krivov & Wyatt 2021, and refs. therein). For example, Krivov & Wyatt (2021)
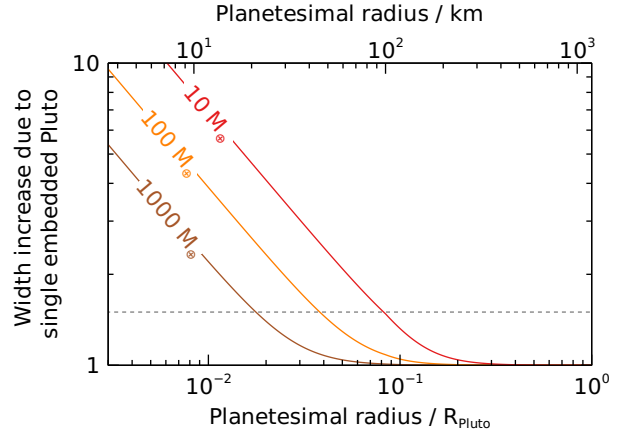

Figure 5. Effect of placing a small fraction of a disc's mass in one Pluto-sized object, where the disc's mass is dominated by smaller objects (Equation 18). The horizontal axis shows the radii of the non-Pluto objects, and the vertical axis the ratio of the disc width with and without the Pluto. Three disc masses are shown, as labelled. The plot shows that a Pluto-sized object could be hidden in a disc dominated by smaller bodies without significantly broadening the disc, provided that the smaller bodies have radii larger than 100 km (for a 10 $M_\oplus$ disc) or 20 km (for a 1000 $M_\oplus$ disc). The horizontal dashed line shows a width ratio of 1.5.

use 2.8 ± 0.1. So if our largest bodies are up to several hundred kilometres then they would still dominate disc mass, in which case our approach would be justified.

However, the upper end of the primordial size distribution may steepen, possibly in the dwarf-planet regime that we are interested in (Schäfer et al. 2017). It is therefore possible that the largest body *does not* dominate total disc mass. In this case, it could be that primordial Plutos *are* present in the disc, if the disc mass is dominated by smaller bodies.

We examine this using analytics. Ida & Makino (1993) studied the eccentricity growth in a disc comprising numerous small bodies and one embedded large body, where all bodies have mass. Their Equation 4.1 includes terms from both small and large bodies, where we neglected large-body terms in Section 3. We now revisit our earlier analysis, this time keeping both their small- and large-body terms, and neglecting the dynamical-friction term of Ida & Makino (1993) using the arguments in their Section 4. Using this, we derive the width ratio of two equivalent-mass discs; one comprising only equal-mass bodies, and one where some mass is in one larger body. If w_{M+m} is the disc width with the larger body and w_m that without, then

$$\frac{w_{M+m}}{w_m} = \left[1 + \frac{M}{m_{\text{disc}}} \left(\frac{2M}{m} - 1 \right) \right]^{1/4}, \quad (18)$$

where M and m are the masses of the larger and smaller bodies respectively. Using this, we calculate the effect of introducing a single embedded Pluto into a disc, as shown on Figure 5.

The plot shows that one Pluto could be hidden in a disc whose mass is dominated by smaller objects, provided the smaller objects are not too small. Specifically, if Fomalhaut's disc mass is dominated by bodies with radii larger than 100 km (for a 10 $M_\oplus$ disc) or 20 km (for a 1000 $M_\oplus$ disc), then an embedded Pluto would not increase the disc width by more than a factor of 1.5. Therefore, whilst we demonstrate that Fomalhaut's disc cannot be dominated by primordial Plutos, a

single Pluto could still be embedded in the disc without significantly broadening it.

This single-Pluto result yields insight into the multi-Pluto case. Additional Plutos would further excite the disc, so Equation 18 (for a single Pluto) is a lower bound for the multi-Pluto case. If embedded Plutos do not excite each other, then the dynamical effect due to multiple Plutos would be roughly linear with their number. This is quantified by multiplying the factor M/m_{disc} in Equation 18 by the number of embedded Plutos, which moves the lines on Figure 5 upwards. Hence, if the disc contains Plutos but the disc mass is dominated by smaller bodies, then the degree of disc broadening increases with the number of Plutos. Furthermore, in reality multiple embedded Plutos would excite each other, so broaden the disc even more. We therefore conclude that primordial Plutos could be embedded in Fomalhaut's disc, but the disc mass must be dominated by smaller bodies.

5.4 Omitting planetesimal growth

We demonstrated that Fomalhaut's primordial disc was not dominated by Plutos, otherwise it would have broadened by now. However, it is possible that planetesimals continued to merge and grow after the protoplanetary disc dissipated, with Plutos forming much more recently. In this case, the younger Plutos might not yet have had time to disrupt the disc, so whilst no Plutos were in the primordial disc, they could be present today.

To test this, we rearrange Equation 5 for time t, and set $s = 1$ R_{Pluto} and $m_{disc,0} = 9 \pm 2$ $M_\oplus$ (the latter from Equation 8). This yields the maximum age that Plutos can have without having disrupted the disc, which is 100 ± 100 Myr. So given the 440 ± 40 Myr of Fomalhaut, if Plutos are present in the disc today, then they must have to have taken at least ~ 300 Myr to form.

Plutos could theoretically form over this timescale; whilst smaller planetesimals are expected to rapidly form via pebble concentration or streaming instability, the subsequent building of Plutos via core accretion can take much longer (Krivov & Booth 2018). By combining Equations 27 and 41 of Kenyon & Bromley 2008, we find that Plutos could form in Fomalhaut's disc over at least 300 Myr, provided that the sub-Plutos were sufficiently unexcited to prevent collisional fragmentation, and the initial planetesimal disc had a surface density less than 5 times the MMSN. This seems reasonable around the 1.92 $M_\odot$ Fomalhaut, so it is possible that, whilst no Plutos existed in the primordial debris disc, they have since formed and will disrupt the disc in future.

In a broader context: collisional models of debris discs typically assume the size distribution evolves with time at intermediate sizes ($\sim s_{km}(t)$), as progressively larger bodies enter the cascade (e.g. Löhne et al. 2008; Krivov & Wyatt 2021). However, if dwarf-planet formation is also ongoing, then the upper end of the distribution should simultaneously evolve away from a primordial slope as larger bodies grow. There should therefore be a size where the cascade transitions from either destruction- or primordial-dominated to growth-dominated. This could be factored into future models, as it has implications for the total disc mass and the self-stirring level.

5.5 Gas drag

Another possibility is that primordial Plutos *are* present in the narrow ring, but that this ring is prevented from spreading by gas drag. This seems unlikely, because the observed-gas content of the Fomalhaut ring is low, especially compared to other A stars (Matrà et al.

2017; Hughes et al. 2018). To test this, we consider two possibilities; either gas confines planetesimals to a narrow ring, or gas confines observed millimetre dust, whilst unseen planetesimals have a wider distribution.

To test the first possibility, we consider planetesimals in a narrow, eccentric gas disc. These planetesimals would interact with gas in the Stokes drag regime, with acceleration $\ddot{\mathbf{r}} \propto -|\mathbf{v}_{rel}|\mathbf{v}_{rel}$ (where $\mathbf{v}_{rel}$ is the planetesimal's velocity relative to the gas). Beaugé et al. (2010) show that, in a non-precessing eccentric disc, gas eventually drives such planetesimals onto narrow, eccentric orbits matching the gas. This occurs over the proper-eccentricity damping timescale. Combining their Equations 4, 18 and 19, we find that a planetesimal's proper eccentricity e_p is damped by gas on a timescale

$$\tau_{e_p} \equiv \frac{e_p}{|\dot{e}_p|} = \frac{32 s \rho(s)}{3 \pi e_p C_D \rho_g} \sqrt{\frac{a}{G m_*}}, \tag{19}$$

where ρ_g is the gas volume density and C_D is a drag coefficient ($C_D = 0.44$ for 1 km planetesimals; Adachi et al. 1976; Weidenschilling 1977).

Applying this to Fomalhaut: the observed CO gas mass has an upper limit $m_g < 4.9 \times 10^{-4}$ $M_\oplus$ (Matrà et al. 2015). If the gas is co-located with the dust, then its density is roughly $\rho_g \approx m_g / [2\pi^2 a_{disc} (\Delta a_{disc}/2)^2] < 8.7 \times 10^{-21}$ g cm^{-3}. If no other gas is present, then Equation 19 shows that a 1 km planetesimal would take at least 1.1×10^{14} yr to damp into a narrow ring, which is far longer than Fomalhaut's 4.4×10^8 yr age. These timescales are even longer for larger planetesimals. There could be more gas in other, undetected species, but Equation 19 shows that at least 100 $M_\oplus$ of gas would be needed to damp planetesimals within Fomalhaut's age. Assuming the unseen gas is predominantly H_2, this requires a CO/H_2 abundance ratio of at most 10^{-7}, which is much lower than typical ISM values of 10^{-4} (e.g. Kóspál et al. 2013; Matrà et al. 2015). Hence it seems unlikely that Fomalhaut's planetesimals are confined to a narrow ring by gas.

The second possibility is that the planetesimal belt is wider than the observed millimetre belt, but that the millimetre dust is confined by a narrow ring of gas. For plausible gas quantities in the Fomalhaut disc, the mean-free path of gas molecules is much larger than 1 mm, regardless of gas species. This means that dust interacts with gas in the Epstein drag regime, with an acceleration of either $\ddot{\mathbf{r}} \propto -\mathbf{v}_{rel}$ or $-|\mathbf{v}_{rel}|\mathbf{v}_{rel}$ if the grain is subsonic or supersonic respectively (e.g. Kwok 1975; Armitage 2010; Pearce et al. 2020). For simplicity we assume the grain is supersonic, to drive maximal damping. In this case $\ddot{\mathbf{r}} \propto -|\mathbf{v}_{rel}|\mathbf{v}_{rel}$ and we can again use the Beaugé et al. (2010) formalism, only the prefactor C in their Equation 4 now becomes $\rho_g / [s \rho(s)]$. This means that Equation 19 is reduced by a factor $8/(3 C_D)$ when applied to supersonic dust.

Substituting numbers for Fomalhaut: if only CO gas is present, then millimetre grains would be damped into a narrow ring over 17 Myr. However, these grains would be destroyed in collisions before damping could complete, over a 1 Myr timescale (Pearce et al. 2021). Yet this raises the possibility that realistic gas masses *could* confine millimetre grains; if observed CO constitutes at most 10 per cent of the total gas mass, then dust could be confined by gas. However, we do not consider this realistic, for two reasons. First, the ring is relatively sharp in ALMA images (MacGregor et al. 2017), with very little millimetre emission either side. If planetesimals actually had a broader distribution, then we would expect some millimetre emission either side of the ring from dust released in planetesimal collisions. This is not observed. Second, gas would also perturb ~ 10 μm grains as they migrated inwards from the belt through Poynting–Robertson drag.

Such grains are seen by the *James Webb Space Telescope* (*JWST*), yet their profile is well explained by a gas-free model (Gáspár et al. 2023; Sommer et al. 2025). We therefore find it unlikely that gas maintains Fomalhaut's narrow ring in the face of dynamical spreading, by either confining planetesimals or dust, so we do not believe that gas affects our overall conclusions.

5.6 Shepherding planets

A final possibility is that the Fomalhaut ring would broaden by itself, but is prevented from doing so by shepherding planets. In this mechanism, planets exert secular torques that repel the ring, so the combined effect of two planets either side of the ring is to confine planetesimals to a narrow range of semimajor axes (e.g. Murray & Dermott 1999).

Goldreich & Tremaine (1979) first proposed shepherding to explain narrow rings of Uranus, which would otherwise broaden through collisions. They argue that a circular, massless, collisionless ring, shepherded by a pair of equal-mass planets at equal distances either side of the ring, would narrow over a timescale

$$t_{\text{shep}} \sim \frac{\Omega_{\text{disc}}^3 a_{\text{disc}} x^5}{f_1 G^2 m_{\text{P}}}, \tag{20}$$

where Ω_{disc} is the disc angular velocity, x the disc-planet separation, m_{P} the planet mass, and f_1 a constant of order 1. They argue that, for a ring in steady state, the shepherding timescale t_{shep} should equal the ring's broadening timescale, which in Uranus' case is the diffusion timescale due to collisions.

For Fomalhaut, the broadening mechanism is self scattering, and the broadening timescale can be estimated from our *n*-body simulations of non-shepherded rings (Section 2). For shepherding planets to counteract scattering and keep the ring narrow, the shepherding timescale from Equation 20 should be at most the broadening timescale from our earlier simulations.

To test this, we run new *n*-body simulations of the Fomalhaut disc plus two shepherding planets. The planets are equal mass, one on either side of the disc, and on coplanar orbits apsidally aligned with the disc. We consider the disc parameters from Figure 2: a 30 $M_\oplus$ disc comprising bodies of radius 1.9 R_{Pluto}, which our *n*-body simulations show would broaden over ~ 20 Myr if not shepherded. We run this simulation three more times, each time including two equal-mass planets of mass 0.7, 0.2 or 0.07 M_{Jup} (200, 70 and 20 $M_\oplus$ respectively), where 0.7 M_{Jup} is the 3σ upper limit near the disc from *JWST* NIRCam (Ygouf et al. 2024). In each case the planets' semimajor axes are calculated using Equation 20, with t_{shep} set to 20 Myr. We set the inner planet's eccentricity to 0.2. We calculate the outer planet's eccentricity such that the forced eccentricity of a test particle at semimajor axis a_{disc} equals the observed disc's forced eccentricity e_{f}, using the two-planet secular analysis in Murray & Dermott (1999). Using these constraints, for planet masses of 0.7, 0.2 and 0.07 M_{Jup} we use inner-planet semimajor axes of 78.9, 102 and 113 au respectively, and the corresponding outer-planet semimajor axes are 194, 171 and 159 au. The outer planet's eccentricities are 0.12, 0.08 and 0.06 respectively. All planet pairs are separated by more than $2\sqrt{3}$ mutual Hill radii, as required for dynamical stability (Chambers et al. 1996), and are initially more than 3 Hill radii from the disc edge to prevent disc scattering (e.g. Gladman 1993; Ida et al. 2000; Kirsh et al. 2009; Pearce et al. 2024).

We find that the shepherded discs still broaden, and even more so than the non-shepherded case. There are two possible reasons for this. First, the planets oscillate in eccentricity due to mutual secular interactions (e.g. Murray & Dermott 1999). As the planets evolve, the forced eccentricity at the disc location changes, so the disc shape also changes. Second, the planets eventually start scattering disc material, which drives the planets towards the disc and thus destabilises the system. This scattering starts when the planets first encounter debris, either as it leaves the disc through debris self-scattering, or as debris orbits change via the above secular interactions. Either way, when the inner planet encounters external debris it starts migrating outwards, and *vice versa* for the outer planet. Hence the planets converge and the intervening disc is broadened. We repeated the shepherding simulations with several other parameters; we varied the disc mass by a factor of 3, the debris-body size by a factor of 2, and the planet locations by 30 per cent in either direction. In all cases, the discs ended up broader than without shepherding.

We conclude that shepherding of Fomalhaut's eccentric disc, if it can occur, would require a delicate balance of system parameters. We were unable to identify a setup where shepherding truly increased the dynamical stability of the system, and the issue is increasingly acute for more massive discs. We note that Boley et al. (2012) did not encounter this problem in their shepherding simulations, because they simulated planets interacting with a massless disc. Whilst we do not conduct a thorough exploration, our simulations suggest that shepherding is difficult to achieve in practise. We therefore believe it unlikely that Fomalhaut's disc contains primordial Plutos, which is prevented from broadening by unseen shepherding planets.

6 DISCUSSION: WIDER IMPACT

We used a new method to show that Fomalhaut's disc mass cannot be dominated by primordial Plutos and that, if Plutos are present, they must have formed recently. This study has wider implications for several areas of debris science, beyond Fomalhaut alone.

First, our conclusion backs up the argument of Krivov & Wyatt (2021), that 'planetesimals are born small' in the brightest debris discs. They argue that the largest bodies must be small, because extrapolating observed dust up to unseen Plutos would mean that the brightest debris discs have masses above 1000 $M_\oplus$, which would violate our understanding of protoplanetary discs (Krivov et al. 2018). Their argument is solely based on collision theory, but here we reach a similar conclusion using dynamics. This means there are now two independent arguments that Plutos are absent from at least some bright debris discs, unless the size distribution turns over sharply at the upper end, or Plutos formed recently.

Second, a major problem in debris science is that we do not know how massive debris discs are. This is because we cannot observe large bodies, which are expected to dominate disc mass. Our paper offers a new technique to dynamically constrain the masses of narrow debris discs. It can easily be applied to other systems, such as HD 53143, HD 181327, and HD 202628, and we intend to incorporate this into a wider study in future. Our analytic methods, such as Equation 5, can be applied without running *n*-body simulations, to constrain disc mass and largest-body size. Note that a disc need not be globally eccentric for our methods to apply; the only requirement is that it is narrow. This manifests as the Δa_{disc}^5 term in Equation 5; if the disc is too wide, then our constraints become significantly weaker.

Our technique adds to a small but growing arsenal of methods to weigh debris discs, which include: using vertical thickness or edge steepness to constrain the masses of stirring bodies (e.g. Ida & Makino 1993; Matrà et al. 2019; Imaz Blanco et al. 2023; Marino 2021), calculating the masses of eccentric discs required to resist planetary shearing (Pearce et al. 2023), using nearby planets to con-

strain the masses of gapped discs from either secular effects (Pearce & Wyatt 2015; Sefilian et al. 2021) or planet migration (Friebe et al. 2022; Booth et al. 2023), and using inclined planets to infer disc masses from vertical structure (Poblete et al. 2023; Sefilian et al. 2025). No single technique can robustly weigh all types of debris disc, so for now, insights must come from targeted constraints using specific methods for specific systems. However, our list of techniques is growing, and expanding our knowledge of debris-disc masses is the thrust of several ongoing works.

7 CONCLUSIONS

We use dynamical models and *n*-body simulations to constrain the largest bodies in the Fomalhaut debris disc. If the bodies were too large, or the disc too massive, then bodies would scatter each other, resulting in a significantly broader disc than observed today. Our main conclusions are:

(i) Primordial Plutos do not dominate the mass of Fomalhaut's debris disc.

(ii) The only way that Plutos could dominate is if they formed recently, within the last 150 Myr (compared to the 440 Myr age of Fomalhaut).

(iii) The only way for primordial Plutos to exist in the disc today is if < 100 km bodies dominate the disc mass.

We investigate many alternative scenarios to maintain the narrow disc, including shepherding planets, collisional damping and gas drag, but find that the above conclusions are robust.

Our paper presents a new method for dynamically constraining debris-disc masses and largest-body sizes, both of which are key unknowns. It provides a new, independent argument that the brightest discs cannot be dominated by large primordial bodies. This provides independent support for Krivov & Wyatt (2021) who, using collisional models, argue that the largest bodies in the brightest debris discs are much smaller than Pluto.

DATA AVAILABILITY

The data underlying this article will be shared upon reasonable request to the corresponding author.

REFERENCES

Abod C. P., Simon J. B., Li R., Armitage P. J., Youdin A. N., Kretke K. A., 2019, ApJ, 883, 192
Adachi I., Hayashi C., Nakazawa K., 1976, Progress of Theoretical Physics, 56, 1756
Anderson J. D., Colombo G., Espsitio P. B., Lau E. L., Trager G. B., 1987, Icarus, 71, 337

Archinal B. A., et al., 2018, Celestial Mechanics and Dynamical Astronomy, 130, 22
Armitage P. J., 2010, Astrophysics of planet formation
Beaugé C., Leiva A. M., Haghighipour N., Otto J. C., 2010, MNRAS, 408, 503
Beust H., et al., 2014, A&A, 561, A43
Boley A. C., Payne M. J., Corder S., Dent W. R. F., Ford E. B., Shabram M., 2012, ApJ, 750, L21
Booth M., et al., 2023, MNRAS, 521, 6180
Bridges F. G., Hatzes A., Lin D. N. C., 1984, Nature, 309, 333
Brown M. E., 2013, ApJ, 767, L7
Brown M. E., Schaller E. L., 2007, Science, 316, 1585
Brozović M., Showalter M. R., Jacobson R. A., Buie M. W., 2015, Icarus, 246, 317
Chambers J. E., Wetherill G. W., Boss A. P., 1996, Icarus, 119, 261
Costa T., Pearce T. D., Krivov A. V., 2024, MNRAS, 527, 7317
Dohnanyi J. S., 1969, J. Geo. Res., 74, 2531
Durda D. D., Dermott S. F., 1997, Icarus, 130, 140
Ernst C. M., Daly R. T., Gaskell R. W., Barnouin O. S., Nair H., Hyatt B. A., Al Asad M. M., Hoch K. K. W., 2023, Earth, Planets and Space, 75, 103
Faramaz V., et al., 2014, A&A, 563, A72
Friebe M. F., Pearce T. D., Löhne T., 2022, MNRAS, 512, 4441
Gáspár A., Rieke G., 2020, Proceedings of the National Academy of Science, 117, 9712
Gáspár A., et al., 2023, Nature Astronomy, 7, 790
Gladman B., 1993, Icarus, 106, 247
Goldreich P., Tremaine S., 1979, Nature, 277, 97
Hahn J. M., 2003, ApJ, 595, 531
Harper D. A., Loewenstein R. F., Davidson J. A., 1984, ApJ, 285, 808
Hayashi C., 1981, Progress of Theoretical Physics Supplement, 70, 35
Hughes A. M., Duchêne G., Matthews B. C., 2018, ARA&A, 56, 541
Ida S., Makino J., 1993, Icarus, 106, 210
Ida S., Larwood J., Burkert A., 2000, ApJ, 528, 351
Imaz Blanco A., et al., 2023, MNRAS, 522, 6150
Jacobson R. A., 2009, AJ, 137, 4322
Jacobson R. A., 2014, AJ, 148, 76
Jacobson R. A., et al., 2006, AJ, 132, 2520
Jankovic M. R., Wyatt M. C., Löhne T., 2024, A&A, 691, A302
Janson M., Carson J. C., Lafrenière D., Spiegel D. S., Bent J. R., Wong P., 2012, ApJ, 747, 116
Johansen A., Mac Low M.-M., Lacerda P., Bizzarro M., 2015, Science Advances, 1, 1500109
Kalas P., et al., 2008, Science, 322, 1345
Kalas P., Graham J. R., Fitzgerald M. P., Clampin M., 2013, ApJ, 775, 56
Kennedy G. M., 2020, Royal Society Open Science, 7, 200063
Kenyon S. J., Bromley B. C., 2008, ApJS, 179, 451
Kirsh D. R., Duncan M., Brasser R., Levison H. F., 2009, Icarus, 199, 197
Kobayashi H., Tanaka H., 2010, Icarus, 206, 735
Konopliv A. S., Banerdt W. B., Sjogren W. L., 1999, Icarus, 139, 3
Kóspál Á., et al., 2013, ApJ, 776, 77
Krivov A. V., 2010, Research in Astronomy and Astrophysics, 10, 383
Krivov A. V., Booth M., 2018, MNRAS, 479, 3300
Krivov A. V., Wyatt M. C., 2021, MNRAS, 500, 718
Krivov A. V., Sremčević M., Spahn F., 2005, Icarus, 174, 105
Krivov A. V., Ide A., Löhne T., Johansen A., Blum J., 2018, MNRAS, 474, 2564
Kwok S., 1975, ApJ, 198, 583
Lockwood A. C., Brown M. E., Stansberry J., 2014, Earth Moon and Planets, 111, 127
Löhne T., Krivov A. V., Rodmann J., 2008, ApJ, 673, 1123
Löhne T., et al., 2012, A&A, 537, A110
MacGregor M. A., et al., 2017, ApJ, 842, 8
Mamajek E. E., 2012, ApJ, 754, L20
Marino S., 2021, MNRAS, 503, 5100
Marino S., 2022, arXiv e-prints, p. arXiv:2202.03053
Matrà L., Panić O., Wyatt M. C., Dent W. R. F., 2015, MNRAS, 447, 3936
Matrà L., et al., 2017, ApJ, 842, 9

Matrà L., Wyatt M. C., Wilner D. J., Dent W. R. F., Marino S., Kennedy G. M., Milli J., 2019, AJ, 157, 135

Matrà L., et al., 2025, A&A, 693, A151

Matthews B. C., Krivov A. V., Wyatt M. C., Bryden G., Eiroa C., 2014, in Beuther H., Klessen R. S., Dullemond C. P., Henning T., eds, Protostars and Planets VI. pp 521–544 (arXiv:1401.0743), doi:10.2458/azu_uapress_9780816531240-ch023

Montesinos B., et al., 2016, A&A, 593, A51

Murray C. D., Dermott S. F., 1999, Solar system dynamics

Najita J. R., Kenyon S. J., Bromley B. C., 2022, ApJ, 925, 45

Nesvold E. R., Kuchner M. J., Rein H., Pan M., 2013, ApJ, 777, 144

O'Brien D. P., Greenberg R., 2003, Icarus, 164, 334

Ohtsuki K., 1999, Icarus, 137, 152

Pan M., Schlichting H. E., 2012, ApJ, 747, 113

Park R. S., et al., 2016, Nature, 537, 515

Pätzold M., et al., 2016, Nature, 530, 63

Pearce T. D., 2024, arXiv e-prints, p. arXiv:2403.11804

Pearce T. D., Wyatt M. C., 2014, MNRAS, 443, 2541

Pearce T. D., Wyatt M. C., 2015, MNRAS, 453, 3329

Pearce T. D., Wyatt M. C., Kennedy G. M., 2015, MNRAS, 448, 3679

Pearce T. D., Krivov A. V., Booth M., 2020, MNRAS, 498, 2798

Pearce T. D., Beust H., Faramaz V., Booth M., Krivov A. V., Löhne T., Poblete P. P., 2021, MNRAS, 503, 4767

Pearce T., et al., 2023, Using planets to dynamically weigh a debris disc for the first time, JWST Proposal. Cycle 2, ID. #3973

Pearce T. D., et al., 2024, MNRAS, 527, 3876

Pitjeva E. V., Pitjev N. P., 2018, Astronomy Letters, 44, 554

Poblete P. P., Löhne T., Pearce T. D., Sefilian A. A., 2023, MNRAS, 526, 2017

Ragozzine D., Brown M. E., 2009, AJ, 137, 4766

Rein H., Liu S. F., 2012, A&A, 537, A128

Rein H., et al., 2019, MNRAS, 485, 5490

Salo H., Ohtsuki K., Lewis M. C., 2018, in Tiscareno M. S., Murray C. D., eds, , Planetary Ring Systems. Properties, Structure, and Evolution. pp 434–493, doi:10.1017/9781316286791.016

Schäfer U., Yang C.-C., Johansen A., 2017, A&A, 597, A69

Schüppler C., Krivov A. V., Löhne T., Booth M., Kirchschlager F., Wolf S., 2016, MNRAS, 461, 2146

Sefilian A. A., Touma J. R., 2019, AJ, 157, 59

Sefilian A. A., Rafikov R. R., Wyatt M. C., 2021, ApJ, 910, 13

Sefilian A. A., Rafikov R. R., Wyatt M. C., 2023, ApJ, 954, 100

Sefilian A. A., Kratter K. M., Wyatt M. C., Petrovich C., Thébault P., Malhotra R., Faramaz-Gorka V., 2025, arXiv e-prints, p. arXiv:2505.09578

Sibthorpe B., Kennedy G. M., Wyatt M. C., Lestrade J. F., Greaves J. S., Matthews B. C., Duchêne G., 2018, MNRAS, 475, 3046

Simon J. B., Armitage P. J., Li R., Youdin A. N., 2016, ApJ, 822, 55

Simon J. B., Armitage P. J., Youdin A. N., Li R., 2017, ApJ, 847, L12

Sommer M., Wyatt M., Han Y., 2025, MNRAS, 539, 439

Tanaka H., Inaba S., Nakazawa K., 1996, Icarus, 123, 450

Thomas P. C., 2010, Icarus, 208, 395

Trilling D. E., et al., 2008, ApJ, 674, 1086

Vizgan D., et al., 2022, ApJ, 935, 131

Weidenschilling S. J., 1977, Ap&SS, 51, 153

Weissman P. R., 1984, Science, 224, 987

Wyatt M. C., 2008, ARA&A, 46, 339

Wyatt M. C., 2020, in Prialnik D., Barucci M. A., Young L., eds, , The Trans-Neptunian Solar System. pp 351–376, doi:10.1016/B978-0-12-816490-7.00016-3

Wyatt M. C., Smith R., Su K. Y. L., Rieke G. H., Greaves J. S., Beichman C. A., Bryden G., 2007, ApJ, 663, 365

Wyatt M. C., Clarke C. J., Booth M., 2011, Celestial Mechanics and Dynamical Astronomy, 111, 1

Ygouf M., et al., 2024, AJ, 167, 26
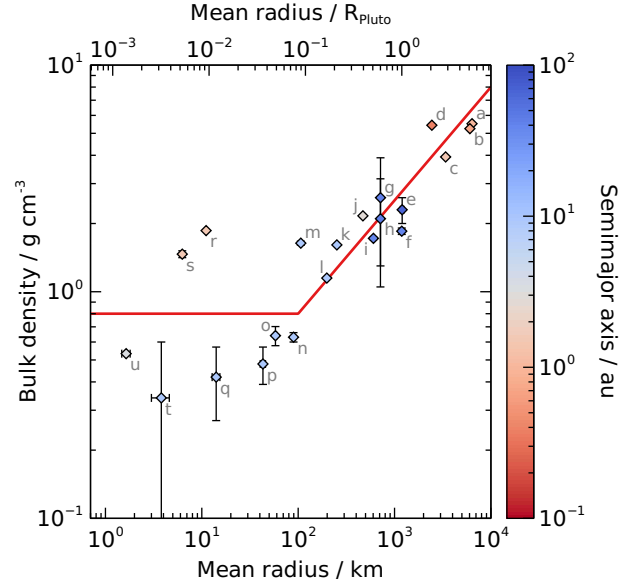
van Leeuwen F., 2007, A&A, 474, 653

Figure A1. Red line: simple approximation for the bulk densities of solid bodies versus their size, as adopted in our *n*-body simulations (Equation 1). Points show various Solar System objects for comparison: [a]Earth, [b]Venus, [c]Mars, [d]Mercury, [e]Eris, [f]Pluto, [g]Haumea, [h]Makemake, [i]Charon, [j]Ceres, [k]Enceladus, [l]Mimas, [m]Phoebe, [n]Janus, [o]Epimetheus, [p]Prometheus, [q]Pan, [r]Phobos, [s]Deimos, [t]Daphnis, [u]Comet 67P. For any data without literature uncertainties, we assume uncertainties of 50 per cent. Colours denote helio-centric semimajor axis; for satellites, this is that of the parent body.

APPENDIX A: BULK DENSITIES OF SOLAR SYSTEM BODIES

We make an approximate relation between debris-body size and bulk density, based on solid bodies in the Solar System. We take sizes and bulk densities from literature[13], and plot these on Figure A1. We then fit (by eye) a simple trend relating bulk density to body size. This is Equation 1, shown by the solid line on Figure A1. Whilst different Solar System bodies have different compositions, so are not expected to follow a single trend, this approximation is good enough for our purposes.

APPENDIX B: SECULAR-RING SIMULATIONS

The *n*-body simulations in Section 2 require prohibitively long computation times for large numbers of particles. We therefore make two assumptions to reduce computational requirements:

(i) That narrow discs comprised of small bodies would remain narrow. This lets us omit *n*-body simulations with very large numbers of particles (lower region of Figure 3).

(ii) That broadened discs would not damp themselves back into narrow rings through self-gravity. This lets us terminate *n*-body simulations early for discs that quickly broaden.

[13] References for Solar System bodies: JPL Solar System Dynamics (https://ssd.jpl.nasa.gov/planets/phys_par.html); Anderson et al. (1987); Konopliv et al. (1999); Jacobson et al. (2006); Brown & Schaller (2007); Jacobson (2009); Ragozzine & Brown (2009); Thomas (2010); Brown (2013); Jacobson (2014); Lockwood et al. (2014); Brozović et al. (2015); Park et al. (2016); Pätzold et al. (2016); Archinal et al. (2018); Ernst et al. (2023).

In this section we verify that both assumptions are valid.

Gravitational interactions can be split into 3 categories: scattering, secular, and mean-motion-resonance interactions. Scattering interactions are close approaches that modify orbits over relatively short timescales; these are what cause discs in our *n*-body simulations to broaden. Conversely, secular interactions occur over much longer timescales.

Full *n*-body simulations include all 3 interactions. As a first test, we continue several *n*-body simulations for long after the discs significantly broaden, and do not detect any later narrowing. These test simulations cover a significant region of the parameter space, and demonstrate that scattering is unlikely to narrow broadened discs.

As a second test we run a different type of simulation, focussing on secular interactions. Secular dominates over scattering if particles are very small (Section 4.1.3 in Costa et al. 2024), or if the interaction occurs over a long time. We therefore use a secular integrator to test our two assumptions above. We describe the techniques below.

B1 Secular integrator

Secular interactions occur on timescales much longer than orbital periods. A disc undergoing secular interactions can therefore be modelled as being composed of ring-like sub belts, where each ring gravitationally interacts with others, causing them to change shape and orientation. To model this, we implement a numerical integrator based on the secular theory below.

To lowest order in eccentricities and inclinations, the orbit-averaged gravitational influence of a set of $N - 1$ perturbers on a particle can be expressed via the disturbing potential

$$\mathcal{R}_i = n_i a_i^2 \sum_{j \neq i} \left[\frac{1}{2} A_{ii} (h_i^2 + k_i^2) + A_{ij} (h_i h_j + k_i k_j) \right] \quad (B1)$$

(e.g. Murray & Dermott 1999). Here the subscript i denotes properties of the particle, j the perturbers, $h \equiv e \sin \varpi$ and $k \equiv e \cos \varpi$ where e and ϖ are eccentricity and longitude of ascending note respectively, a is the semimajor axis, $n_i \equiv \sqrt{G(m_* + m_i) a_i^{-3}}$ is the mean motion, and m is the mass. The values A_{ii} and A_{ij} are elements of the interaction matrix $\mathbf{A}$, where

$$A_{ij} = \begin{cases} \sum_{k \neq i} \frac{n_j m_k}{M_* + m_j} \frac{f(\alpha_{ik})}{4} & \text{if } i = j, \\ -\frac{n_i m_j}{M_* + m_i} \frac{g(\alpha_{ij})}{4} & \text{if } i \neq j. \end{cases} \quad (B2)$$

Here the functions $f = f(\alpha_{ij}, H)$ and $g = g(\alpha_{ij}, H)$ represent the softened Laplace coefficients as introduced by Hahn (2003), where $\alpha_{ij} \equiv a_i/a_j$ for all combinations of a_i and a_j. The softening parameter H can be associated with the relative vertical thickness of a disc, $H \approx \Delta z/r$, accounting for the fact that the local interactions between neighbouring orbits are fundamentally different from that in an infinitely thin disc (see Sefilian & Touma 2019 for a review). We set $H = 0.06$ for narrow belts and $H = 0.15$ for wide belts, although these choices have no significant influence on our conclusions.

In vector notation, the resulting secular changes to the orbital elements of all interacting particles follow from Lagrange's planetary equations

$$\dot{\mathbf{h}} = \mathbf{A}\mathbf{k} \quad \text{and} \quad \dot{\mathbf{k}} = -\mathbf{A}\mathbf{h}, \quad (B3)$$

where $\mathbf{h} \equiv (h_1, ..., h_N)$ and $\mathbf{k} \equiv (k_1, ..., k_N)$ (Murray & Dermott 1999). Up to this point our implementation of the *N*-ring approach

is identical to the models presented by Hahn (2003) and Sefilian et al. (2023), the results of which can be reproduced exactly. Our approach to a numerical solution differs only in that we first decouple Equations B3 into separate sets of undamped harmonic oscillators for *h* and *k* by a second application of $\mathbf{A}$:

$$\ddot{\mathbf{h}} = -\mathbf{A}^2\mathbf{h} \quad \text{and} \quad \ddot{\mathbf{k}} = -\mathbf{A}^2\mathbf{k}. \quad (B4)$$

The eigenvalues and eigenvectors to $-\mathbf{A}^2$ are then sought with the C++ EIGEN library, and when combined with initial conditions $h_i(t = 0)$ and $k_i(t = 0)$, result in time-dependent solutions

$$h_i = \sum_{j=1}^{N} b_{ij} \sin(c_j t + d_j) \quad \text{and} \quad k_i = \sum_{j=1}^{N} b_{ij} \cos(c_j t + d_j) \quad (B5)$$

with amplitudes b_{ij}, frequencies c_j and phase shifts d_j. This solution is valid for an arbitrary time t, and the solution is bounded unless additional perturbers induce secular resonances, where one or several of the amplitudes b_{ij} diverge (Sefilian et al. 2023).

We implement the above theory to model the evolution of 1000 massive sub belts, where each sub belt represents the orbits of bodies in a disc. For a given setup, we calculate the system architecture due to secular interactions at time t using Equation B5. We use this to make the two tests below.

B2 Conclusion 1: narrow secular discs do not broaden

Our first test is whether a narrow disc comprising an ~infinite number of ~infinitesimally small bodies would broaden over time. Such a disc would be entirely secular. We model this using the secular code, considering 12 discs with logarithmically spaced masses between 0.1 and 3000 $M_\oplus$. Each disc comprises 1000 sub-belts, set up with the same parameters as the initial orbits in our *n*-body simulations (Section 2.1). The secular simulations are run for the 440 Myr age of Fomalhaut, and an example simulation with the highest disc mass is shown on the left panel of Figure B1.

None of these stimulations show any significant broadening, and the mean free and forced eccentricities remain very close to their initial values. We can therefore conclude that, for our parameter space, secular effects do not cause narrow discs to broaden. This validates our decision to omit *n*-body simulations of discs with large numbers of small particles; these discs would not broaden over time. These discs do exhibit global precession, but they maintain their global eccentricity and width.

B3 Conclusion 2: broadened secular discs do not narrow

Our second test is whether a broadened disc would damp itself back into a narrow ring through secular effects. We again use the secular code to model 12 discs with logarithmically spaced masses between 0.1 and 3000 $M_\oplus$. We use a similar setup as in Appendix B2, except with a much broader disc (semimajor axes spanning 70 to 200 au), with orbits that are much more excited (proper eccentricities spanning $0 \leq e_p \leq 0.3$). This corresponds to the state of *n*-body simulations where the disc has broadened to ~5 times its initial value. The secular simulations are again run for 440 Myr, and an example for the highest disc mass is shown on the right panel of Figure B1.

Again, no simulations produce a significant change in the global disc morphology. This confirms that, for our parameter space, a broadened debris disc will not become narrow through secular effects. This validates our decision to terminate *n*-body simulations
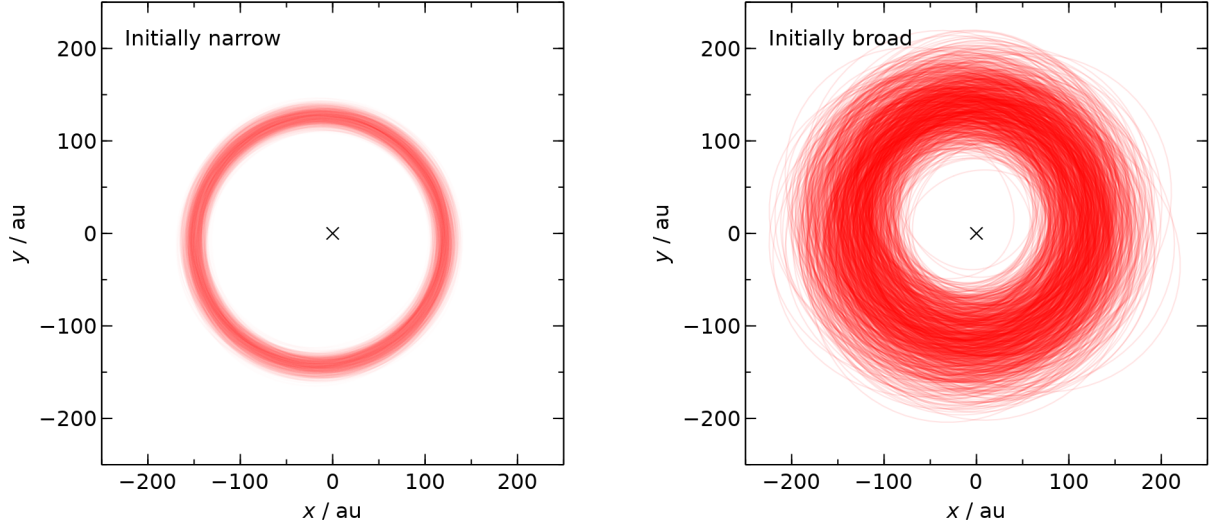
Figure B1. Secular simulations of two 3000 $M_\oplus$ debris discs, each shown at 440 Myr (Appendix B). The cross marks the star, and each red ring is an interacting sub-belt. Left panel: an initially narrow, eccentric disc, with the same initial setup as the Fomalhaut disc (Section 2.1). Right panel: an initially broad, eccentric disc. Each disc maintains its initial global eccentricity and width throughout the simulation, and the results are qualitatively identical for all tested disc masses (0.1 to 3000 $M_\oplus$). This demonstrates that secular effects would not cause our narrow discs to broaden, nor our broadened discs to narrow.

early if the disc significantly broadens, because such a broad disc would remain broad.

APPENDIX C: TREE-GRAVITY TEST

To verify our REBOUND tree-gravity simulations, we compare two batches of test simulations, one using tree gravity and the other simple n-body gravity. We run 12 setups of the Fomalhaut disc, each with 300 debris bodies, with disc masses logarithmically spaced between 0.03 and 10^4 $M_\oplus$. For each setup we run two simulations, one using tree and one using n-body gravity, and compare the resulting disc widths (as measured using the method in Section 2.2). The results are shown on Figure C1.

The tree and n-body simulations show very similar behaviour, with both predicting little disc broadening for disc masses below ~ 10 $M_\oplus$ and then increasing for higher masses. At these high masses, tree gravity yields slightly narrower discs than n-body gravity, but the results deviate by less than 25 per cent, which is not enough to affect our analyses. We therefore conclude that our tree-gravity setup is valid.
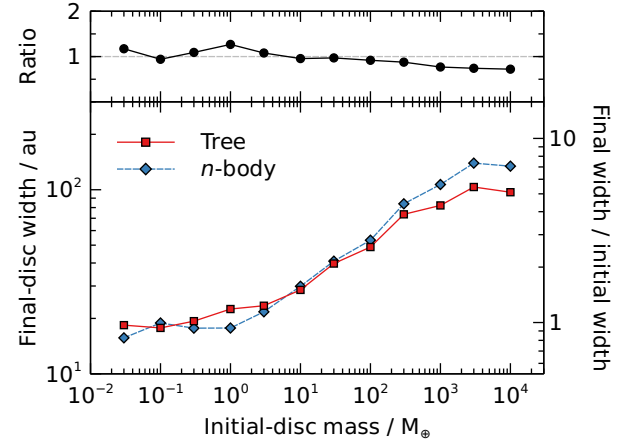

Figure C1. Comparison of simulations using tree gravity to those using simple n-body gravity (Appendix C). Bottom panel: disc widths measured at the end of each simulation, for tree gravity (squares) and n-body gravity (diamonds). Top panel: ratio of disc widths from tree gravity to n-body gravity. Each simulation has 300 debris bodies, and the setups are the same for each gravity type. Each pair of disc widths are within 25 per cent of each other, validating our tree-gravity setup. The turnover at high disc masses is due to our method struggling to fit very broadened discs, whose profiles deviate strongly from Gaussian.

APPENDIX D: COLLISIONAL FUNCTIONS

The functions $f(e,i)$ and $G(q,s,r)$ in Equation 10 are defined in Löhne et al. (2008) as

$$f(e,i) = \sqrt{\frac{5}{4}e^2 + i^2} \tag{D1}$$

and

$$G(q,s,r) \equiv \left[X_c(s,r)^{5-3q} - \left(\frac{s_{max}}{s}\right)^{5-3q} \right]$$
$$+ 2\frac{q-5/3}{q-4/3} \left[X_c(s,r)^{4-3q} - \left(\frac{s_{max}}{s}\right)^{4-3q} \right]$$
$$+ \frac{q-5/3}{q-1} \left[X_c(s,r)^{3-3q} - \left(\frac{s_{max}}{s}\right)^{3-3q} \right], \tag{D2}$$

where

$$X_c(s,r) \equiv \left[\frac{2Q_D^*(s,r)r}{f^2(e,I)\mathcal{G}m_*} \right]^{1/3}.$$

(D3)

This paper has been typeset from a TEX/LATEX file prepared by the author.